

Dragging spin-orbit-coupled solitons by a moving optical lattice

Hidetsugu Sakaguchi¹, Fumihide Hirano¹, and Boris A. Malomed^{2,3}

¹*Department of Applied Science for Electronics and Materials,
Interdisciplinary Graduate School of Engineering Sciences,
Kyushu University, Kasuga, Fukuoka 816-8580, Japan and*

²*Department of Physical Electronics, School of Electrical Engineering,
Faculty of Engineering, and Center for Light-Matter Interaction,
Tel Aviv University, P.O. Box 39040 Tel Aviv, Israel*

³*Instituto de Alta Investigación, Universidad de Tarapacá, Casilla 7D, Arica, Chile*

It is known that the interplay of the spin-orbit-coupling (SOC) and mean-field self-attraction creates stable two-dimensional (2D) solitons (ground states) in spinor Bose-Einstein condensates. However, SOC destroys the system's Galilean invariance, therefore moving solitons exist only in a narrow interval of velocities, outside of which the solitons suffer delocalization. We demonstrate that the application of a relatively weak moving optical lattice (OL), with the 2D or quasi-1D structure, makes it possible to greatly expand the velocity interval for stable motion of the solitons. The stability domain in the system's parameter space is identified by means of numerical methods. In particular, the quasi-1D OL produces a stronger stabilizing effect than its full 2D counterpart. Some features of the domain are explained analytically.

Keywords: matter waves; lattice potentials; soliton mobility; semi-vortices; mixed modes; Galilean boost; delocalization

I. INTRODUCTION

The spin-orbit coupling (SOC) is a fundamental effect in physics of semiconductors, induced by the interaction of the electron's spin with the magnetic field produced by the Lorentz transform of the electrostatic field of the crystalline lattice in the reference frame moving along with the electron [1–3]. While in the solid-state settings SOC is a complex phenomenon, it has been demonstrated that it may be emulated in a much simpler form in binary atomic Bose-Einstein condensates (BECs). The experiments have realized the SOC emulation in BEC by mapping the spinor wave function of electrons into the two-component (pseudo-spinor) wave function of the atomic condensate [5–7]. In terms of coupled Gross-Pitaevskii equations (GPEs), which provide a very accurate dynamical model for BEC in the mean-field approximation [4], SOC, i.e., the coupling of the momentum and pseudospin of the matter waves, is represented by linear terms with first spatial derivatives which mix two components of the spinor wave function [8, 9].

Many theoretical works addressed the interplay of SOC with the intrinsic nonlinearity of BEC, which represents, in the mean-field approximation, effects of collisions between atoms in the dilute quantum gas. In the case of the self-attractive sign of the nonlinearity, the analysis has predicted the modulational instability [10] and various species of one-dimensional (1D) solitons [11]–[21] under the action of SOC. In the case of the repulsive nonlinearity, the use of spatially periodic optical-lattice (OL) potentials has made it possible to predict 1D gap solitons [22, 23, 25]. Otherwise, the interplay of SOC with self-repulsion gives rise to families of dark solitons [26]–[30].

While most experimental realizations of SOC were reported in the effectively 1D geometry, SOC has also been created in the 2D setting [31]. Theoretical analyses of 2D setups, including SOC and the intrinsic repulsive nonlinearity, addressed vortices [32]–[35], monopoles [36], skyrmions [37, 38], and other delocalized states. In the presence of the OL potential and self-repulsion, 2D gap solitons were predicted too [39]. The lattice potential can also stabilize 2D SOC solitons in the case of self-attraction [40]. Another possibility to create stable 2D solitons is offered by the higher-order (beyond-mean-field) self-repulsion in BEC components [41], or by long-range dipole-dipole interactions [42, 43].

As concerns settings based on GPEs with the mean-field cubic self-attraction in the free 2D space, originally it was believed that all self-trapped states generated by these models, such as Townes solitons [44], are completely unstable, as the same setting gives rise to the critical collapse which leads to destruction of solitons by perturbations [45–47]. Nevertheless, it has been found that the addition of the usual linear SOC of the Rashba [2] type is sufficient to suppress the collapse and create otherwise missing ground states in the linearly coupled system of GPEs with the cubic attractive terms [48]. Then, the same result was produced [49] by the consideration of the binary system linearly coupled by a combination of the Rashba and Dresselhaus [1] SOC terms. This possibility to stabilize 2D solitons was further elaborated in Refs. [50]–[53], see also a brief review in [54].

There are two different species of 2D solitons supported by the attractive nonlinearity in the two-component SOC system, in cases when ratio γ of the strength of the attraction between the components to the strength of the self-

attraction in each component is $\gamma < 1$ or $\gamma > 1$. In the former case, the 2D system produces stable *semi-vortex* (SV) solitons as the ground state, in which one component has zero vorticity, and the other one carries vorticity 1. On the other hand, the ground state of the system with $\gamma > 1$ is represented by *mixed modes* (MMs), which are composed of terms with zero and nonzero vorticities in both components (therefore they called “mixed”) [48]. Simultaneously, SVs and MMs exist but are unstable at $\gamma > 1$ and $\gamma < 1$, respectively.

Mobility of solitons in SOC systems is an issue of straightforward physical interest [20]. It is a nontrivial property because SOC terms break the Galilean invariance [11, 48, 55]. By means of numerical methods, it was found [48, 52] that SVs and MMs may stably move only in one direction in the 2D plane (note that SOC destroys the system’s isotropy too), with velocity v_0 taking values in a finite interval,

$$0 \leq v_0 < (v_{\max})_{\text{SV,MM}}. \quad (1)$$

At $v_0 = v_{\max}$, the soliton disappears through delocalization. The critical velocity v_{\max} takes moderate values for MMs, being very small for SVs. This observation is explained by the fact the SV’s structure is actually incompatible with the mobility, see details below.

A possibility to enhance mobility of solitons is to drag them by means of a moving OL potential, which is an experimentally available tool [56, 57]. In this work we aim to elaborate this option and demonstrate that the moving OL with a relatively small amplitude is able to stabilize the motion of the 2D solitons up to much higher values of the velocity than in the free space. The model and a relevant analytical framework are presented in Section II. Systematic results, obtained, chiefly, by means of numerical methods are reported in Section III. In particular, for the dragged SVs, the increase of v_0 leads, first, to their transformation into MMs, while the delocalization takes place at much higher velocities. Considering both the full 2D lattice and its quasi-1D counterpart, we conclude that the latter one produces an *essentially stronger* stabilizing effect on the moving solitons than the full 2D lattice. Moreover, a surprising result is that the strongest stabilization is provided by the quasi-1D lattice with the wave vector directed *perpendicular to the velocity*. This finding is explained by the fact that such a lattice suppresses delocalization of the moving soliton in the transverse direction. The paper is concluded by Section IV.

II. THE MODEL AND ANALYTICAL FRAMEWORK

A. The basic equations

Following Ref. [48], we consider the system of coupled GPEs for two components $\phi_{\pm}(x, y, t)$ of the BEC spinor wave function written in the laboratory reference frame. The equations include, as the first option, a square-shaped OL potential $U_{2\text{D}}(x, y; t)$ with amplitude U_0 and wavenumbers q , moving at velocity v_0 along the y direction in the (x, y) plane:

$$\begin{aligned} i\frac{\partial\phi_+}{\partial t} &= -\frac{1}{2}\nabla^2\phi_+ - (|\phi_+|^2 + \gamma|\phi_-|^2)\phi_+ \\ &\quad - U_{2\text{D}}(x, y; t)\phi_+ + \lambda\left(\frac{\partial\phi_-}{\partial x} - i\frac{\partial\phi_-}{\partial y}\right), \end{aligned} \quad (2)$$

$$\begin{aligned} i\frac{\partial\phi_-}{\partial t} &= -\frac{1}{2}\nabla^2\phi_- - (|\phi_-|^2 + \gamma|\phi_+|^2)\phi_- \\ &\quad - U_{2\text{D}}(x, y; t)\phi_- - \lambda\left(\frac{\partial\phi_+}{\partial x} + i\frac{\partial\phi_+}{\partial y}\right), \end{aligned} \quad (3)$$

$$U_{2\text{D}}(x, y; t) = U_0 \cos(qx) \cos(q(y - v_0t)). \quad (4)$$

In this notation, \hbar and the atomic mass, as well as the effective coefficient of the self-attraction in each component, are scaled to be 1, while $\gamma \geq 0$ is the above-mentioned ratio of the cross/self interaction strengths, and $\lambda > 0$ is the real coefficient of SOC of the Rashba type.

Parallel to the full 2D potential (4), we consider its quasi-1D variants, with the wave vector oriented parallel or perpendicular to the velocity:

$$U_{1\text{D}}(y; t) = U_0 \cos(q(y - v_0t)); U_{1\text{D}}(x) = U_0 \cos(qx). \quad (5)$$

In the latter case, the quasi-1D OL is not actually moving (but the solitons will move in the y direction), therefore Eqs. (2) and (3) with potential $U_{1\text{D}}(x)$ do not explicitly depend on time. Using the remaining scaling invariance of Eqs. (2) and (3) (which includes a freedom of rescaling the coordinated by an arbitrary factor), in most cases we fix

$$q = 2\pi/3 \quad (6)$$

in potentials (4) and (5), which is a value convenient for numerical simulations. Nevertheless, some results for other values of q are presented below too, see Eqs. (40) and (42). Including results in this form is relevant because in the experiment it is possible to change the period of the OL, keeping other parameters fixed [58].

It is relevant to mention that, in the framework of the usual GPE with cubic self-attraction, 2D solitons may be stabilized not only by the full 2D spatially periodic potential [59–62], but also by its quasi-1D version [63], see also Ref. [64]. Furthermore, in the free 2D space, solitons can be stabilized by the SOC terms taken in an essentially quasi-1D form [53]. Somewhat surprisingly, the present analysis reveals, in the next section, that the quasi-1D potentials (5), especially $U_{1D}(x)$, provide an essentially stronger stabilizing effect for moving solitons than the full 2D potential.

In the moving reference frame with coordinate $\tilde{y} = y - v_0 t$, Eqs. (2) and (3) are rewritten as

$$\begin{aligned} i\frac{\partial\phi_+}{\partial t} - iv_0\frac{\partial\phi_+}{\partial\tilde{y}} &= -\frac{1}{2}\nabla^2\phi_+ - \left(|\phi_+|^2 + \gamma|\phi_-|^2\right)\phi_+ \\ &\quad - U_{2D}(x, \tilde{y}; t)\phi_+ + \lambda\left(\frac{\partial\phi_-}{\partial x} - i\frac{\partial\phi_-}{\partial\tilde{y}}\right), \end{aligned} \quad (7)$$

$$\begin{aligned} i\frac{\partial\phi_-}{\partial t} - iv_0\frac{\partial\phi_-}{\partial\tilde{y}} &= -\frac{1}{2}\nabla^2\phi_- - \left(|\phi_-|^2 + \gamma|\phi_+|^2\right)\phi_- \\ &\quad - U_{2D}(x, \tilde{y}; t)\phi_- - \lambda\left(\frac{\partial\phi_+}{\partial x} + i\frac{\partial\phi_+}{\partial\tilde{y}}\right), \end{aligned} \quad (8)$$

$$U_{2D}(x, \tilde{y}) = U_0 \cos(qx) \cos(q\tilde{y}), \quad (9)$$

$$U_{1D}(\tilde{y}) = U_0 \cos(q\tilde{y}); U_{1D}(x) = U_0 \cos(qx). \quad (10)$$

In particular, Eqs. (7) and (8) with $U_{2D} = 0$ admit a family of continuous-wave (CW) solutions with arbitrary amplitude A and wavenumber k_y (for the definiteness' sake, we here assume $k_y > 0$):

$$\begin{aligned} (\phi_{\pm}(\tilde{y}, t))_{CW} &= \pm A \exp(ik_y\tilde{y} - i\mu_{CW}t), \\ \mu_{CW} &= k_y^2/2 - k_y(\lambda + v_0) - A^2. \end{aligned} \quad (11)$$

Signs \pm in front of the components of this solution are chosen to select the CW branch with lower energy.

Soliton solutions to Eqs. (7) and (8) with the OL potential (9) or (10) and chemical potential μ are looked for in the usual form,

$$\phi_{\pm}(x, y, t) = u(x, y) \exp(-i\mu t). \quad (12)$$

These solutions, along with the respective values of μ , were obtained by means of the imaginary-time evolution method [65–67] applied to Eqs. (7) and (8) for a fixed value of the total norm,

$$N = \int \int \left(|\phi_+(x, y)|^2 + |\phi_-(x, y)|^2\right) dx dy, \quad (13)$$

as the method is adjusted for finding solutions under this condition.

Even if the above equations are not invariant with respect to the Galilean transform, for analytical considerations it is useful to rewrite them in the moving reference frame, applying the formal Galilean boost to Eqs. (7) and (8):

$$\phi_{\pm} \equiv \exp\left(iv_0\tilde{y} + \frac{i}{2}v_0^2t\right) \tilde{\phi}(x, \tilde{y}, t). \quad (14)$$

The accordingly transformed system is

$$\begin{aligned} i\frac{\partial\tilde{\phi}_+}{\partial t} &= -\frac{1}{2}\nabla^2\tilde{\phi}_+ - \left(|\tilde{\phi}_+|^2 + \gamma|\tilde{\phi}_-|^2\right)\tilde{\phi}_+ \\ &\quad - U_{2D}(x, \tilde{y}; t)\tilde{\phi}_+ + \lambda\left(\frac{\partial\tilde{\phi}_-}{\partial x} - i\frac{\partial\tilde{\phi}_-}{\partial\tilde{y}}\right) + \lambda v_0\tilde{\phi}_-, \end{aligned} \quad (15)$$

$$\begin{aligned} i\frac{\partial\tilde{\phi}_-}{\partial t} &= -\frac{1}{2}\nabla^2\tilde{\phi}_- - \left(|\tilde{\phi}_-|^2 + \gamma|\tilde{\phi}_+|^2\right)\tilde{\phi}_- \\ &\quad - U_{2D}(x, \tilde{y}; t)\tilde{\phi}_- - \lambda\left(\frac{\partial\tilde{\phi}_+}{\partial x} + i\frac{\partial\tilde{\phi}_+}{\partial\tilde{y}}\right) + \lambda v_0\tilde{\phi}_+, \end{aligned} \quad (16)$$

Unlike Eqs. (7) and (8), this system includes direct inter-component mixing with coefficient λv_0 , but does not include the group-velocity terms, $-iv_0\partial\phi_{\pm}/\partial\tilde{y}$.

B. Analytical estimates

Knowledge of the spectrum of the linearized set of equations (15) and (16) without the potential ($U_0 = 0$) helps one to predict the existence region for solitons. A straightforward calculation for small-amplitude excitations, taken as

$$\tilde{\phi}_{\pm} \sim \exp(ik_x x + ik_y y - i\tilde{\mu}t), \quad (17)$$

yields two branches of the dispersion relation between chemical potential μ and wave vector (k_x, k_y) ,

$$\tilde{\mu} = \frac{1}{2}k^2 \pm \lambda \sqrt{k_x^2 + (k_y + v_0)^2}. \quad (18)$$

Expression (18) takes values in the propagation band,

$$\tilde{\mu} \geq \tilde{\mu}_{\min} \equiv -\lambda^2/2 - |\lambda v_0|, \quad (19)$$

while solitons may populate the remaining semi-infinite bandgap, $\tilde{\mu} < \tilde{\mu}_{\min}$. Note that the increase of the velocity pushes μ_{\min} down, thus reducing the bandgap. All the soliton solutions produced indeed satisfy the condition $\tilde{\mu} < \tilde{\mu}_{\min}$.

It is relevant to mention that the 1D limit of Eqs. (15), (16) and (10), corresponding to no x dependence and potential $U_0 \cos(q\tilde{y})$, admits an obvious substitution,

$$\tilde{\phi}_{\pm}(\tilde{y}, t) = \exp(-i\lambda\tilde{y} + i(\lambda^2/2 - \lambda v_0)t) \phi(\tilde{y}, t), \quad (20)$$

with which the system reduces to the single equation:

$$i \frac{\partial \phi}{\partial t} = -\frac{1}{2} \frac{\partial^2 \phi}{\partial \tilde{y}^2} - (1 + \gamma) |\phi|^2 \phi - U_0 \cos(q\tilde{y}) \phi. \quad (21)$$

Evidently, Eq. (21) is the usual 1D GPE with the standard OL potential, which always has soliton solutions [58], hence this 1D limit, unlike the full 2D system, admits the motion of solitons with an unlimited velocity.

Coming back to the 2D system, a crude explanation for the existence of the limit value of the velocity, v_{\max} (see Eq. (1)), may be proposed, based on the numerical observation that, close to the delocalization transition at $v_0 = v_{\max}$, the solitons are, quite naturally, very broad in the x direction, keeping weakly separated maxima in the two components (see Fig. 1 below), i.e., they feature splitting of the components. This observation suggests to address a possibility of the splitting in terms of the stationary version of Eqs. (15) and (16) for constant-amplitude solutions with chemical potential $\tilde{\mu} < 0$:

$$\tilde{\phi}_{\pm} = \tilde{u}_{\pm} \exp(-i\tilde{\mu}t), \quad (22)$$

where amplitudes \tilde{u}_{\pm} may be real, and (close to the center) $U_{2D}(x, \tilde{y})$ is replaced by U_0 :

$$(\tilde{\mu} + U_0) \tilde{u}_+ + (\tilde{u}_+^2 + \gamma \tilde{u}_-^2) \tilde{u}_+ - \lambda v_0 \tilde{u}_- = 0, \quad (23)$$

$$(\tilde{\mu} + U_0) \tilde{u}_- + (\tilde{u}_-^2 + \gamma \tilde{u}_+^2) \tilde{u}_- - \lambda v_0 \tilde{u}_+ = 0. \quad (24)$$

Then, it is relevant to look for a critical point at which a solution with an infinitesimal splitting between the components, $\Delta\tilde{u} \equiv \tilde{u}_+ - \tilde{u}_-$, appears on top of the obvious solution to Eqs. (23) and (24) with identical (unsplit) components,

$$\tilde{u}_{\pm}^2 = -(\tilde{\mu} + U_0 - \lambda v_0) / (1 + \gamma). \quad (25)$$

A simple calculation, based on equations (23) and (24) linearized with respect to $\Delta\tilde{u}$, yields the value of v_0 at the critical point:

$$v_{\max} = (1 - \gamma) (\tilde{\mu} + U_0) / (2\lambda), \quad (26)$$

the splitting being impossible at $v_0 > v_{\max}$. Finally, the substitution of value (26) in Eq. (25) yields the background amplitude at the critical point, $\tilde{u}_{\pm}^2 = -(\tilde{\mu} + U_0)/2$. Because the delocalization transition proceeds via small-amplitude solitons (see Fig. 1 below), the present consideration is relevant for small $|\tilde{\mu} + U_0|$ and, naturally, for small values of the SOC strength, λ , to justify the use of the constant-amplitude solution. The prediction of the delocalization

point, given by Eq. (26), makes sense at $\gamma < 1$, and it does not apply at $\gamma > 1$, when the formal expression predicts a negative velocity.

This consideration reveals the possibility of the splitting between the components which is only qualitatively similar to what occurs in the solitons of the MM type. Therefore, it is relevant to compare dependence $v_{\max} = \text{const} \cdot \lambda^{-1}$, predicted by Eq. (26), with numerical results (see the dashed hyperbola in Fig. 5(b) below), fitting const to the numerical data, rather than using the coefficient from Eq. (26).

In the limit of large λ , opposite to one considered above, v_{\max} can be estimated using the variational approximation (VA). To simplify the matters, one may apply it to the 1D limit of Eqs. (15) and (16), in which the y derivatives are dropped (this limit case is opposite to one considered above in the form of Eqs. (20) and (21), where the x derivatives were omitted). The stationary version of these equations for real functions $\tilde{u}_{\pm}(x)$, defined as in Eq. (22), is

$$\left[\tilde{\mu} + U_{1D}(x) + \frac{1}{2} \frac{d^2}{dx^2} + \tilde{u}_+^2 + \gamma \tilde{u}_-^2 \right] \tilde{u}_+ + \lambda \left(v_0 - \frac{d}{dx} \right) \tilde{u}_- = 0, \quad (27)$$

$$\left[\tilde{\mu} + U_{1D}(x) + \frac{1}{2} \frac{d^2}{dx^2} + \tilde{u}_-^2 + \gamma \tilde{u}_+^2 \right] \tilde{u}_- + \lambda \left(v_0 + \frac{d}{dx} \right) \tilde{u}_+ = 0, \quad (28)$$

Because, in the case of large λ , the delocalization always happens with states of the MM type, one may use the following Gaussian ansatz for mirror-symmetric components of the wave function:

$$(\tilde{u}_{\pm}(x))_{\text{ans}} = A \exp \left(-\frac{(x \mp \xi)^2}{2W^2} \right), \quad (29)$$

where A and W are the amplitude and width, 2ξ being the separation between the split peaks of the components. The full form of VA turns out to be cumbersome, but, in the limit of large λ , the prediction for $(v_0)_{\max}$, as the critical value at which the solution for W , with a fixed value of the norm, becomes impossible, is simple: $(v_0)_{\max} = \lambda$ (this approximation neglects the presence of the potential). The particular coefficient in this expression depends on the assumptions adopted to apply VA, but the linear form of the dependence,

$$(v_0)_{\max} = \text{const} \cdot \lambda, \quad (30)$$

is a corollary of scaling properties of Eqs. (15) and (16), in the absence of the external potential (the scaling leaves the total norm (13) of the 2D system invariant). The scaling is corroborated in detail below by a typical numerical solution displayed in Fig. 4. Equation (30) explains, approximately or exactly, numerical findings presented below in Figs. 5(a) and 8.

We note, in passing, that the linearized version of Eqs. (27) and (28) with the 1D potential (10) admits a parametric resonance, accounted for by solutions in the form of

$$\tilde{u}_{\pm}(x) = a_{\pm} \cos \left(\frac{q}{2} x \right) + b_{\pm} \sin \left(\frac{q}{2} x \right) \quad (31)$$

Straightforward consideration of Eqs. (27) and (28) demonstrates that the parametric resonance takes place at

$$\tilde{\mu} = \frac{q^2}{2} \pm \sqrt{\left(\lambda \frac{q}{2} \right)^2 + \left(\lambda v_0 \pm \frac{U_0}{2} \right)^2}, \quad (32)$$

where the two signs \pm are mutually independent. However, the parametric resonance does not play an essential role in this work.

III. RESULTS

As mentioned above, stationary 2D soliton solutions were produced by means of the imaginary-time integration of Eqs. (7) and (8), performed for a fixed total norm (13) of the solitons. It was then verified by systematic simulations of perturbed evolution of the solitons in real time that they are stable in the respective existence intervals (1). The identification of v_{\max} is the main objective of the numerical analysis. For the system of Eqs. (7) and (8) with $\gamma = 0$ and $\gamma = 2$, we report the results with $N = 5$ and 3, respectively, as these values make it possible to present generic results. Numerical computations were performed in the 2D domain of size 12×12 , which is sufficient to display all details of the 2D soliton profiles.

A. Dragging 2D solitons by the square-shaped OL in the absence of the nonlinear cross-interaction ($\gamma = 0$)

Results for the system with $\gamma = 0$ in Eqs. (2) and (3), when, as mentioned above, only SVs are relevant solutions at $v_0 = 0$, are presented in Figs. 1 – 6. These results are produced for the full 2D lattice, defined as per Eq. (4), with amplitude U_0 (some figures display the results for $U_0 = 0$).

First, a set of cross sections of the moving solitons, corresponding to gradually increasing velocities, are displayed in Fig. 1. Panel (a) represents, for the sake of comparison, the results for the free space ($U_0 = 0$), which corresponds to Ref. [48]. This set of profiles demonstrates that, with the increase of v_0 , the SV, which exists at $v_0 = 0$, is gradually transformed into a soliton with a quasi-MM structure. Indeed, linear-mixing terms $\sim \lambda v_0$ in the system written in the form of Eqs. (15) and (16) make the existence of pure SVs, whose components carry different vorticities, 0 and 1, impossible. The growth of the mixing terms, with the increase of v_0 , tends to make the two components mutually mirror-symmetric. The transition to this shape, which is the signature of the MM structure, occurs in Fig. 1(a) at

$$v_0 = v_{\text{SV} \rightarrow \text{MM}}(U_0 = 0) \approx 0.25. \quad (33)$$

Simultaneously, the soliton expands in the x direction, and eventually disappears, through complete delocalization, at

$$v_{\text{max}}(U_0 = 0) \approx 0.65. \quad (34)$$

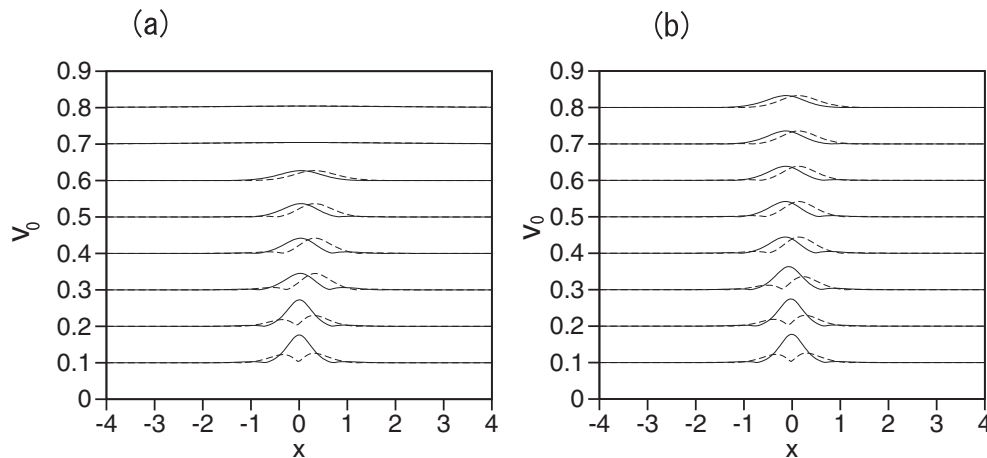


FIG. 1: (a) Solid and dashed lines show cross-section plots of $|\phi_+(x)|$ and $|\phi_-(x)|$ at $y = 0$ for 2D solitons moving in the free space ($U_0 = 0$), under the action of SOC with strength $\lambda = 3$ in Eqs. (15) and (16). Values of the velocity, v_0 , are marked in the panel. (b) The same for the solitons dragged by the square-shaped potential (4) with amplitude $U_0 = 0.5$ and velocity v_0 . The results are obtained for the solitons with fixed norm $N = 5$, setting $\gamma = 0$ (the nonlinear cross-interaction is absent).

Figure 1(b) displays similar results, produced by the imaginary-time-simulation method in the moving reference frame in the presence of the square-shaped OL potential (9) with a relatively small amplitude, $U_0 = 0.5$. In this case, the SV \rightarrow MM and delocalization transitions occur at, respectively,

$$v_{\text{SV} \rightarrow \text{MM}}(U_0 = 0.5) \approx 0.32, \quad (35)$$

$$v_{\text{max}}(U_0 = 0.5) \approx 1.75. \quad (36)$$

cf. Eqs. (33) and (34). It is seen that the effect of the OL potential is small in terms of the former transition, and quite strong for the expansion of the existence region of the moving solitons. In addition, Fig. 2 shows the full 2D shape of the solitons by means of contour plots of $|\phi_-(x, y)|$ at $v_0 = 0.2$ (a) and 0.4 (b) for $U_0 = 0$. In particular, the plots clearly show the presence of a vortex-antivortex pair at $v_0 = 0.4$, which is a characteristic feature of patterns of the MM type, and is not possible in SVs.

The results for $U_0 = 0$ and 0.5 are further detailed in Fig. 3. Panel (a) shows the peak value A of squared component $|\phi_+|^2$ as a function of the velocity. In the delocalized state, the peak amplitude does not fall to zero, because of the

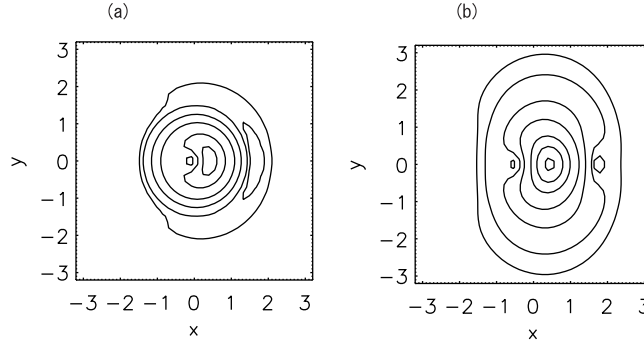


FIG. 2: Contour plot of $|\phi_-(x,y)|$ at $v_0 = 0.2$ (a) and 0.4 (b) for the solitons at $U_0 = 0$. The contour lines are plotted for $|\phi_-| = 0.05, 0.1, 0.25, 0.5, 1, 1.5, 2$.

finite system's size. Further, the SV \rightarrow MM transition is quantified in panel (b) by plots of the parameter characterizing the asymmetry between the two components,

$$R \equiv N^{-1} \iint |\phi_+(x,y)|^2 dx dy - 1/2, \quad (37)$$

vs. the velocity for $U_0 = 0$ and 0.5 (here N is the total norm defined as per Eq. (13)). For MM solitons, whose components are mirror images of each other, $R = 0$, while one has $R > 0$ for SVs. Figure 3(b) clearly demonstrates the SV \rightarrow MM transition at points (33) and 35) for $U_0 = 0$ and 0.5 , respectively. Further, Fig. 3(c) shows the relationship between chemical potential μ of the solitons (see Eq. (12)) and velocity v_0 for the same soliton families. The dashed line is the chemical potential of the delocalized CW state at $U_0 = 0$, as given by Eq. (11), in which constant A^2 is expressed in terms of N , and $k_y = 2\pi \cdot 7/L$ is chosen. The chain of rhombuses coinciding with the CW line at $v_0 > v_{\max}(U_0 = 0) \approx 0.65$ (see Eq. (34)) represents fully delocalized states.

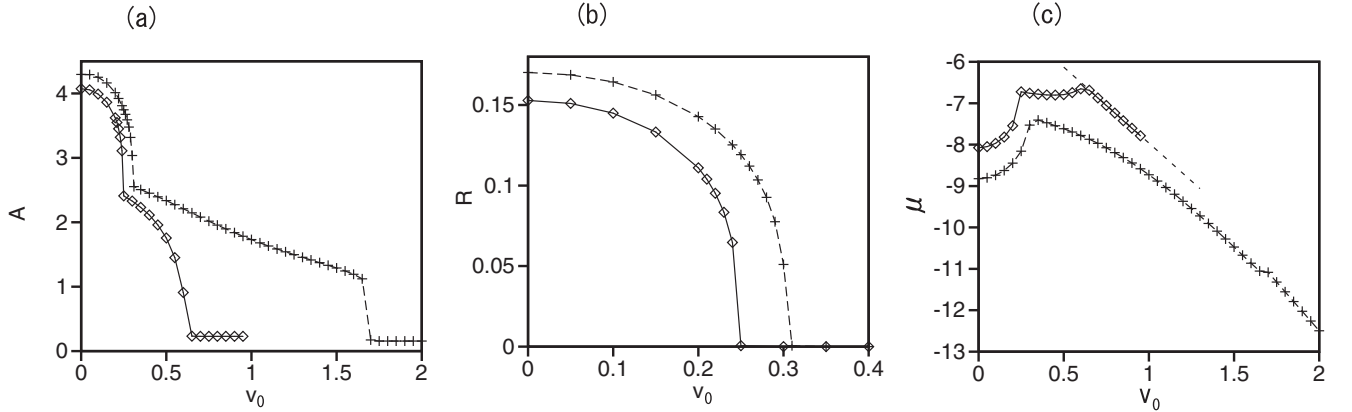


FIG. 3: (a) Peak values A of squared component $|\phi_+|^2$ of the moving solitons, as functions of the velocity, v , in the free space ($U_0 = 0$, shown by rhombuses), and under the action of the 2D lattice potential (9) with $U_0 = 0.5$, shown by crosses. (b) The asymmetry parameter (37) vs. v for the same soliton families. (c) The chemical potential vs. v_0 for same families. The dashed line, plotted as per Eq. (11) with $k_y = 2\pi \cdot 7/L$, represents the fully delocalized CW state. The solutions are obtained with $\lambda = 3$ and $\gamma = 0$ in Eqs. (2) and (3). The fixed norm of the solitons is $N = 5$.

To verify the above-mentioned scaling which links different soliton solutions of Eqs. (7) and (8) with $U_0 = 0$, we note that, if a spinor wave function $\phi_{\pm}(x, \tilde{y}, t)$ is a solution for parameters $\{\lambda, v_0, \gamma\}$, then a solution for the set of $\{s\lambda, sv_0, \gamma\}$ is given by

$$\phi_{\pm}^{(s)} = s\phi_{\pm}(sx, s\tilde{y}, s^2t; s\lambda, sv_0), \quad (38)$$

where s is an arbitrary scaling factor. To check this property, Fig. 4 shows $|\phi_+|$ and $|\phi_-|$ (solid and dashed lines, respectively) for the numerically found soliton solutions with (a) $\{\lambda = 3, v_0 = 0.2\}$ and (b) $\{\lambda = 1.5, v_0 = 0.1\}$, which

corresponds to $s = 0.5$ in Eq. (38). To check relation (38) in detail, Fig. 4(c) compares $|\phi_{\pm}|$ (with both components drawn by solid lines) for the former solution and the rescaled version of the latter one, $2|\phi_{2\pm}|$ (dashed lines), plotted in rescaled coordinates, $x' = 0.5x, y' = 0.5y$. The overlap of the profiles confirms scaling relation (38) and, consequently, the linear relation,

$$(v_0)_{\max}(s\lambda) = s(v_0)_{\max}(\lambda) \quad (39)$$

for $U_0 = 0$.

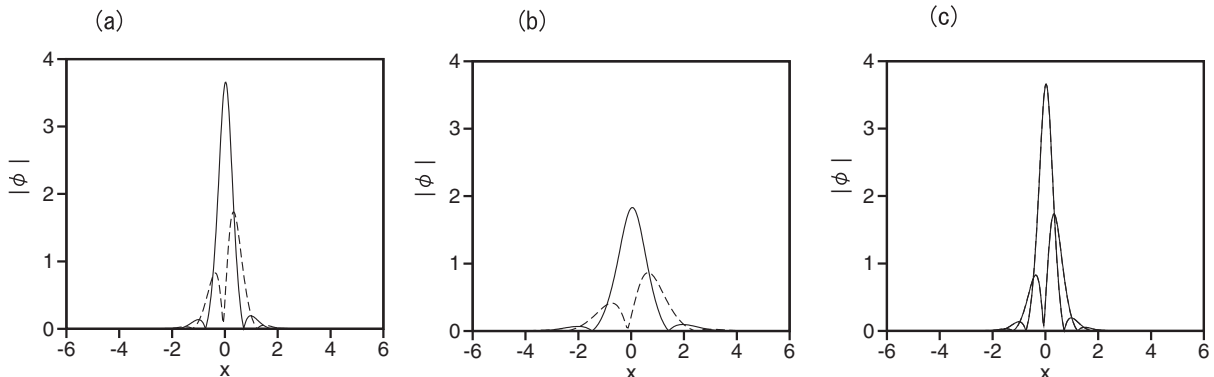


FIG. 4: (a) Profiles of cross sections $|\phi_+(x)|$ and $|\phi_-(x)|$ (solid and dashed lines, respectively) of the stationary solutions of Eqs. (7) and (8) with $\lambda = 3$, $v_0 = 0.2$, and $U_{2D} = 0$. (b) The same at $\lambda = 1.5$ and $v_0 = 0.1$. (c) Juxtaposition of $|\phi_{\pm}(x)|$ from (a) (solid lines) with rescaled profiles $2|\phi_{\pm}^{(s)}(x')|$ from (b) (dashed lines), plotted in rescaled coordinates $x' = 0.5x, y' = 0.5y$. The superimposed profiles completely overlap.

As seen below in Figs. 5(b) and 8(b), the presence of the moving lattice breaks the exact linearity of Eq. (39), but keeps it as an approximate dependence between $(v_0)_{\max}$ and λ . The slope of the approximately linear dependence is strongly affected by the lattice – actually, helping to expand the existence domain of the moving solitons.

The findings produced by the numerical solution for the solitons dragged by the 2D lattice are summarized in Fig. 5 by diagrams which display existence regions of the 2D solitons of the SV and MM types in the parameter plane of (λ, v_0) for $U_0 = 0.5$ (a), and in the plane of (U_0, v_0) for a fixed value of the SOC strength, $\lambda = 1.5$ (b). In these plots, symbol 0 implies the delocalization (nonexistence of solitons). The MM area appears in Fig. 5(a) at $\lambda > 0.75$. Again, these plots demonstrate that the effect of the OL potential is weak for the SV \rightarrow MM transition, and strong for the expansion of the solitons' existence range.

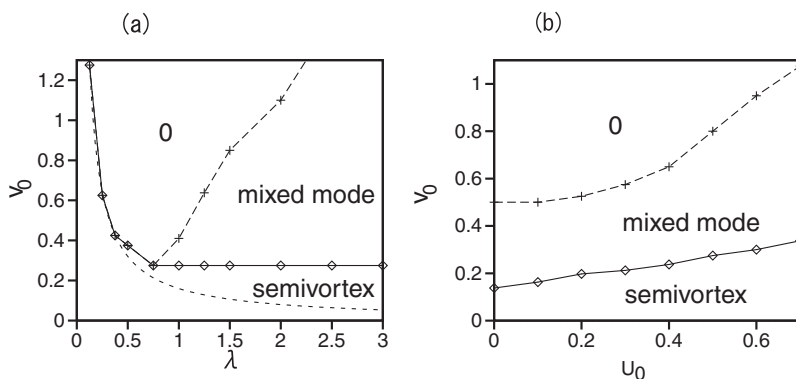


FIG. 5: (a) Existence regions for SVs and MMs in the plane of the SOC strength, λ , and velocity v_0 , in the presence of the square-shaped potential (9) with amplitude $U_0 = 0.5$. Symbol 0 designates the delocalization area, where solitons do not exist. The dashed line in (a) is hyperbola $v_0 = 0.16/\lambda$, which verifies analytical prediction (26), with the fitting coefficient 0.16. Panel (b) shows the existence regions in the plane of the potential's strength, U_0 , and velocity v_0 , for a fixed SOC strength, $\lambda = 1.5$. The results are obtained for $\gamma = 0$ (no nonlinear interaction between the two components) and the fixed norm of the solitons, $N = 5$.

The shape of the left boundary between the SV and 0 areas in Fig. 5(a) is qualitatively explained by Eq. (26), as shown by the dashed hyperbola, drawn with a fitting coefficient 0.16. As said above, this approximation is relevant only for small values of the SOC strength, λ , therefore it does not apply to other boundaries in Figs. 5(a) and (b). On the other hand, the roughly linear shape of the MM-delocalization boundaries is explained, as mentioned above, by the scaling relation (30).

To verify robustness of solutions for the solitons pulled by the moving OL, we have also performed direct real-time simulations of equations (2) and (3) written in the laboratory reference frame. As initial conditions, we used stationary solutions which were obtained, as above, by means of the imaginary-time integration in the coordinates moving at a certain velocity, $(v_0)_{\text{init}}$, while Eqs. (2) and (3) were simulated in real time with the 2D potential moving at a higher (final) velocity, $(v_0)_{\text{fin}} > (v_0)_{\text{init}}$.

As a result, one might expect, in principle, to observe nonstationary solitons traveling at some mean speed $\langle v \rangle < (v_0)_{\text{fin}}$, so that they lag behind the dragging OL. However, our simulations have not produced such solutions. Instead, in all cases when $(v_0)_{\text{fin}}$ belongs to the stability areas shown in Fig. 5, the initial solitons either pick up the speed $(v_0)_{\text{fin}}$, moving with some internal vibrations, or suffer destruction. Characteristic examples are displayed in Fig. 6. As expected according to Fig. 5(b), the initial soliton, corresponding to $(v_0)_{\text{init}} = 0.1$, and the established one, with $(v_0)_{\text{fin}} = 0.2$ in panel (a), belong to the SV type, while the soliton eventually traveling at $(v_0)_{\text{fin}} = 0.3$ in (b) is of the MM type. Finally, setting $(v_0)_{\text{fin}} = 0.5$ in (c) leads to destruction of the soliton (delocalization), due to the large mismatch between $(v_0)_{\text{fin}}$ and $(v_0)_{\text{init}}$. Residual intrinsic vibrations of the established solitons are illustrated by oscillations of asymmetry factor $R(t)$ (defined above in Eq. (37)), which are displayed in Fig. 6(d). The oscillations are nearly regular, keeping $R > 0$ (i.e., the soliton keeps the asymmetry between its components, which is a signature of SVs) for $(v_0)_{\text{fin}} = 0.2$, or irregular, oscillating around $R = 0$, for the MM observed at $(v_0)_{\text{fin}} = 0.3$. The regular oscillations in the case of the semivortex are, essentially, performed by the "lighter" vortex component of the SV moving around the "heavier" zero-vorticity one. The compound soliton of the mixed-mode (MM) type actually has a larger number of effective degrees of freedom, as its both components have equal "masses" (norms), and each component features sub-units with zero and nonzero vorticities. Therefore, the structure of the MM soliton opens a way to observe more complex internal dynamics.

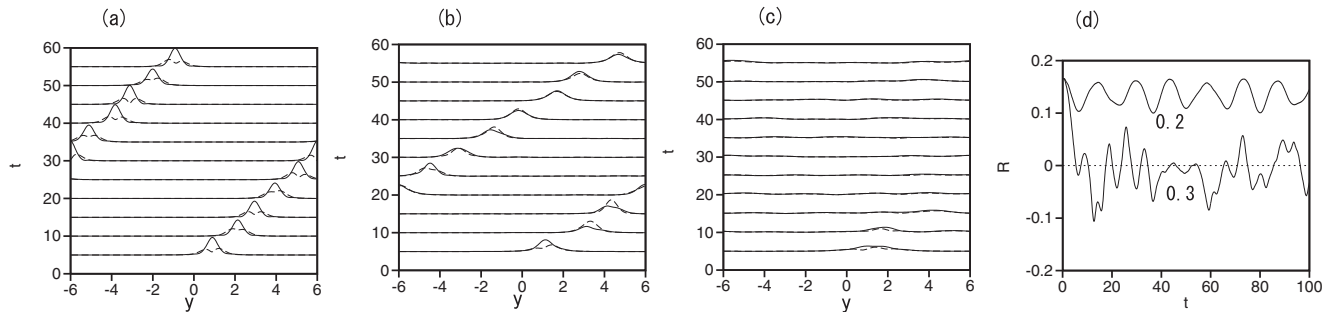


FIG. 6: (a) Solid and dashed lines display the evolution of $|\phi_+(y,t)|$ and $|\phi_-(y,t)|$ in cross section $x = 0$, as produced by simulations of the propagation governed by Eqs. (2) and (3) with $\lambda = 3$, $\gamma = 0$, and $U_0 = 0.5$. The input is taken as the stationary soliton with norm $N = 5$ and velocity $(v_0)_{\text{init}} = 0.1$, while the velocity in Eqs. (2) and (3) is $(v_0)_{\text{fin}} = 0.2$ in (a), 0.3 in (b), and 0.5 in (c). (d) The evolution of asymmetry parameter (37) corresponding to $(v_0)_{\text{fin}} = 0.2$ and 0.3, i.e., to panels (a) and (b), respectively.

B. Dragging and steering solitons by quasi-1D potentials

Proceeding to results obtained from Eqs. (15) and (16) with U_{2D} replaced by quasi-1D potentials (10), Fig. 7(a) shows the corresponding characteristics of the soliton families defined as in Fig. 3, i.e., the peak value A of $|\phi_+|^2$ as a function of v_0 . First, we notice that, if the 2D potential is replaced by $U_{1D}(\tilde{y})$, with the same amplitude and wavenumber as above, $U_0 = 0.5$ and $q = 2\pi/3$, the largest velocity, up to which the quasi-1D potential can drag the soliton, increases from the value given by Eq. (36) to $v_{\text{max}} \approx 2.25$.

A characteristic example of the longitudinal structure of the stable soliton dragged by potential $U_{1D}(\tilde{y})$ is displayed in Fig. 7(b) (in the transverse x direction, the soliton features a smooth localized shape). A dominant wavenumber related to this multi-peak structure is $k_y \simeq 4.6$. It is relevant to note that this value is very different from $q/2 = \pi/3 \approx 1.05$ (see Eq. (6)), which is one that may be, in principle, singled out by the condition of the parametric resonance

induced by terms $U_0 \cos(q\tilde{y}) \tilde{\phi}_\pm$ in Eqs. (15) and (16), cf. Eqs. (31) and (32). Thus, the dynamical mechanisms considered in this work are not affected by the possibility of the resonance.

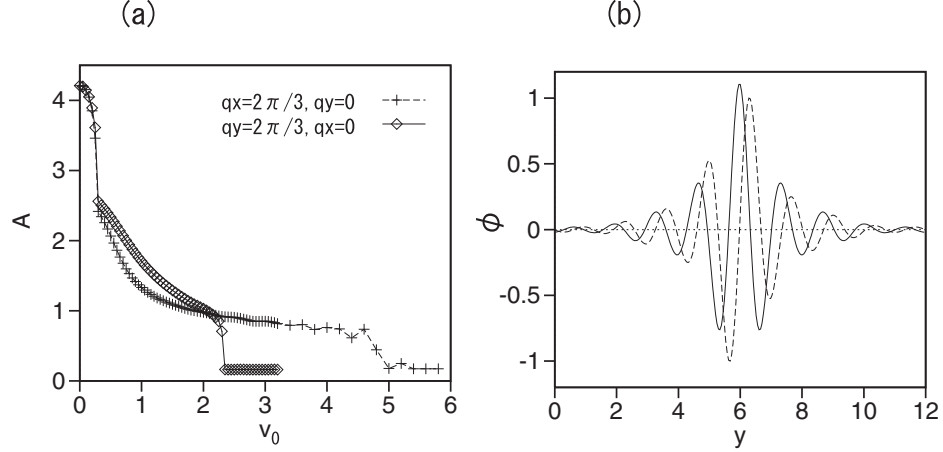


FIG. 7: (a) The same as in Fig. 3(a) with $U_0 = 0.5$, but under the action of the quasi-1D potentials (10). The data labeled “ $qx = 2\pi/3, qy = 0$ ” and “ $qy = 2\pi/3, qx = 0$ ” correspond, respectively, to potentials $U_{1D}(x)$ and $U_{1D}(\tilde{y})$. (b) Snapshot profiles of the wave-function components $\text{Re}(\phi_+)$ and $\text{Im}(\phi_+)$, in cross section $x = 0$, for the soliton with $v = 1.5$, pulled by the moving potential $U_{1D}(\tilde{y})$.

On the other hand, if the quasi-1D potential is taken as $U_{1D}(x)$ in Eq. (10), once again with the same amplitude and wavenumber as above, the highest velocity admitting stable motion of the solitons (which are actually not dragged, but steered along the guiding channel, in such a case) is much larger. Indeed, Fig. 6(a) produces $v_{\max} \approx 5$ for the solitons traveling under the action of potential $U_{1D}(x)$. This value is, roughly, *three times* larger than its counterpart (36) obtained above in the case of the 2D potential. The steep increase of v_{\max} in the latter case is explained by the fact that the potential $U_{1D}(x)$ tends to compress the 2D system of Eqs. (15) and (16) into its 1D version. In turn, the 1D system may be reduced, as mentioned above, to the single GPE (21), which has no limitation for the existence of solitons at any velocity.

The increase of v_{\max} following the replacement of the 2D lattice by the quasi-1D ones has also been checked for the lattice wavenumbers different from value (6) which was fixed above. It was thus found that

$$q = 5\pi/6 : v_{\max}^{(2D)} = 1.225, v_{\max}^{(1D,y)} = 1.525, v_{\max}^{(1D,x)} = 3.175, \quad (40)$$

$$q = 2\pi/3 : v_{\max}^{(2D)} = 1.75, v_{\max}^{(1D,y)} = 2.25, v_{\max}^{(1D,x)} \approx 5, \quad (41)$$

$$q = \pi/2 : v_{\max}^{(2D)} \approx 3.2, v_{\max}^{(1D,y)} \approx 5.4, v_{\max}^{(1D,x)} \approx 13.35, \quad (42)$$

respectively, for $U_{2D}(x, y)$, $U_{1D}(y)$, and $U_{1D}(x)$. Here, for the sake of comparison, Eq. (41) reproduces the above-mentioned results for $q = 2\pi/3$. It is seen that, in all the cases, v_{\max} decreases with the increase of q . This trend is naturally explained by the fact that the convolution of the soliton’s wave function with the rapidly oscillating OL potential produces a weaker effect.

C. Dragging MM solitons in the presence of the nonlinear cross-interaction ($\gamma > 1$)

As said above, the quiescent ($v_0 = 0$) ground-state solutions of Eqs. (2) and (3) with $\gamma > 1$ in the free space ($V_0 = 0$) are MM solitons, while the SVs are unstable in this case. Then, the 2D potential (9) can drag the MMs up to the respective limit velocity, v_{\max} , above which the solitons suffer delocalization. First, the boundary between the moving MMs and delocalized states in the free space ($U_0 = 0$) is plotted in Fig. 7(a) for the system with $\gamma = 2$. The linear shape of the boundary is rigorously explained by Eq. (30) which follows from the scaling properties of Eqs. (2) and (3) with $U_0 = 0$ and a fixed norm. Next, the same boundary, but in the presence of the dragging potential, is plotted in Fig. 7(b). It is seen that even relatively weak potentials, with $U_0 = 0.2$ and 0.4 , help to strongly expand the stability area for the moving MM solitons.

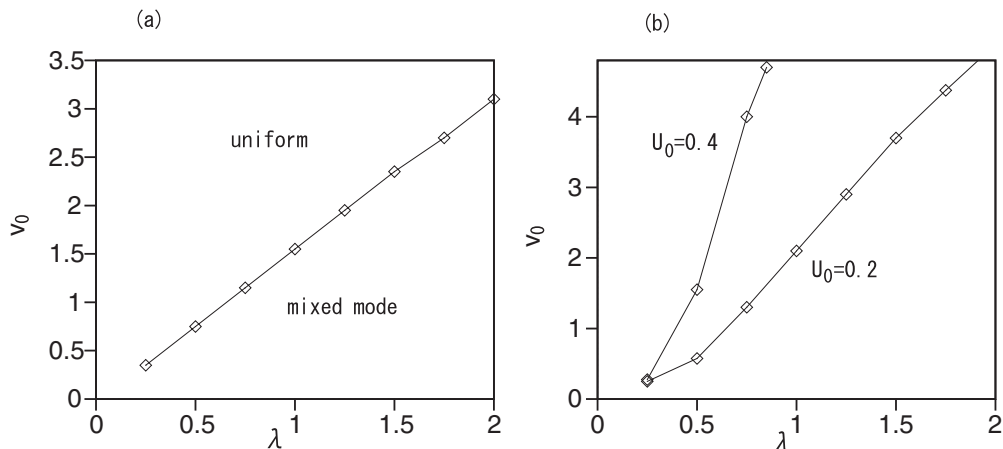


FIG. 8: (a) The boundary between the MMs moving in the free space ($U_0 = 0$) and the delocalized (uniform) state, in the plane of (λ, v) . (b) The same, in the presence of the 2D potential (9) with $U_0 = 0.2$ and 0.4 . The data are presented for the system with $\gamma = 2$ and a fixed norm of the MM solitons, $N = 3$.

IV. CONCLUSION

In this work, we have demonstrated that mobility limits for two-component 2D matter-wave solitons, stabilized by the SOC effect, may be strongly expanded by means of relatively weak spatially periodic potentials moving at a desirable speed. Boundaries of the stable motion are identified by means of numerical methods, and the shape of some boundaries is explained analytically. If the stable quiescent solitons are SVs (semivortices), the motion converts them into MMs (mixed modes), which suffer delocalization at much higher velocities. A remarkable finding is that quasi-1D potentials, especially the one with the wave vector directed perpendicular to the velocity, provide essentially stronger stabilization than the full 2D lattice.

The analysis reported here may be extended to develop schemes for the transfer of a soliton by a moving potential from an initial position to a predetermined final one, cf. Refs. [69–71]. Further, it may be interesting to develop the analysis for two- and multi-soliton complexes trapped in the lattice potential. A challenging option, suggested by Ref. [68], is to consider a possibility to stabilize 3D moving solitons, which are made metastable by SOC in the quiescent state.

Acknowledgments

This was supported, in part, by the Israel Science Foundation through grant No. 1286/17, and by the Japan Society for the Promotion of Science KAKENHI (Grant No. 18K03462)

ORCID IDs

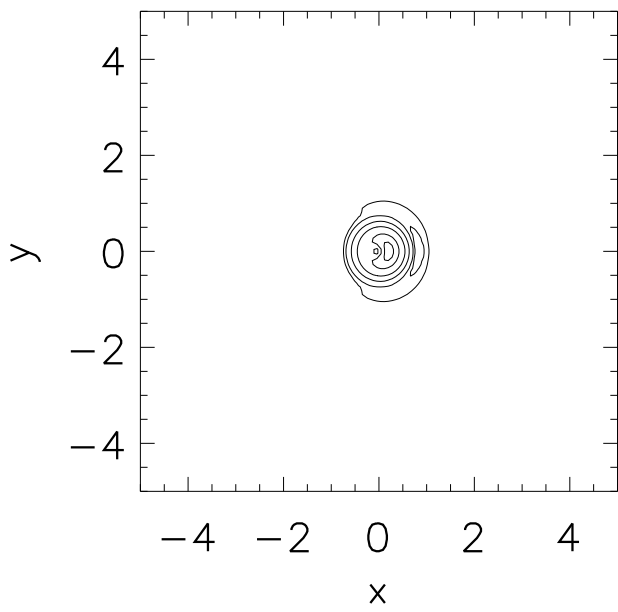
B. A. Malomed 0000-0001-5323-1847; H. Sakaguchi 0000-0003-3591-0496

-
- [1] Dresselhaus G, Spin-orbit coupling effects in zinc blende structures, 1955 *Phys Rev* **100** 580-586
[2] Bychkov Y A and Rashba E I, Oscillatory effects and the magnetic susceptibility of carriers in inversion layers, 1984 *J. Phys. C* **17** 6039-6045
[3] Wu M W, Jiang J H and Weng M Q, Spin dynamics in semiconductors, 2010 *Phys. Rep.* 493 61-236
[4] Pitaevskii L and Stringari S, *Bose-Einstein Condensation* (Oxford University Press: Oxford, UK, 2003)
[5] Lin Y J, Jimenez-Garcia K and Spielman I. B., Spin-orbit coupled Bose - Einstein condensates, 2011 *Nature* **471** 83-86
[6] Zhang J. -Y., Ji S. -C., Chen Z, Zhang L, Du Z. -D., Yan B, Pan G.-S., Zhao B, Deng Y.-J., Zhai H, Chen S and Pan J.-W., Collective dipole oscillations of a spin-orbit coupled Bose-Einstein condensate, 2012, *Phys. Rev. Lett.* **109** 115301

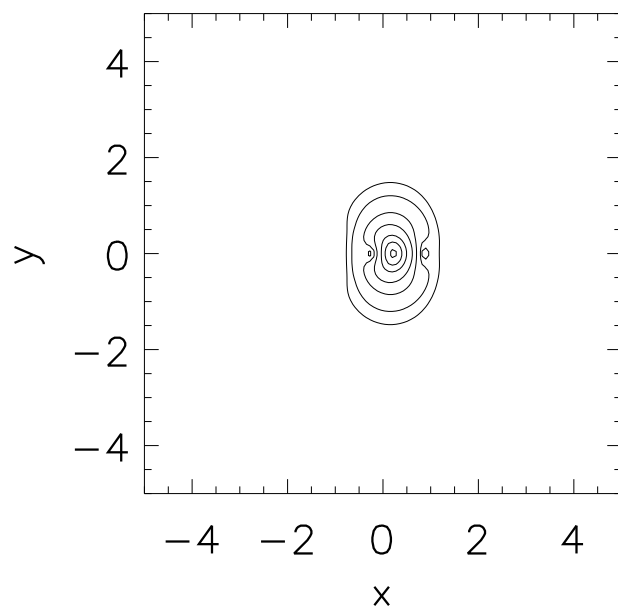
- [7] Campbell D. L., Juzeliūnas G and Spielman I. B., Realistic Rashba and Dresselhaus spin-orbit coupling for neutral atoms, 2011 *Phys. Rev. A* **84**, 025602
- [8] Galitski V and Spielman I B, Spin-orbit coupling in quantum gases 2013 *Nature* **494** 49-54
- [9] Zhai H, Degenerate quantum gases with spin-orbit coupling: a review 2015 *Rep. Prog. Phys.* **78** 026001
- [10] Bhat I A, Mithun T, Malomed B A and Porsezian K, Modulational instability in binary spin-orbit-coupled Bose-Einstein condensates, 2015 *Phys. Rev. A* **92** 063606
- [11] Xu Y, Zhang Y and Wu B, Bright solitons in spin-orbit-coupled Bose-Einstein condensates, 2013 *Phys. Rev. A* **87**, 013614
- [12] Salasnich L and Malomed B A, Localized modes in dense repulsive and attractive Bose-Einstein condensates with spin-orbit and Rabi couplings 2013 *Phys. Rev. A* **87** 063625
- [13] Achilleos V, Frantzeskakis D J, Kevrekidis P J and Pelinovsky D E, Matter-wave bright solitons in spin-orbit coupled Bose-Einstein condensates 2013 *Phys. Rev. Lett.* **110** 264101
- [14] Liu Y-K and Yang S-J, Exact solitons and manifold mixing dynamics in the spin-orbit-coupled spinor condensates 2014 *EPL* **108** 30004
- [15] Kartashov Y V, Konotop V V and Zezyulin D A, Bose-Einstein condensates with localized spin-orbit coupling: Soliton complexes and spinor dynamics 2014 *Phys. Rev. A* **90** 063621
- [16] Peotta S, Mireles F and Di Ventra M, Edge binding of sine-Gordon solitons in spin-orbit-coupled Bose-Einstein condensates 2015 *Phys. Rev. A* **91**, 021601(R) (2015).
- [17] Beličev P, Gligorić G, Petrović J, Maluckov A, Hadžievski L and Malomed B, Composite localized modes in discretized spin-orbit-coupled Bose-Einstein condensates 2015 *J. Phys. B At. Mol. Opt. Phys.* **48** 065301
- [18] Gautam S and Adhikari S K, Mobile vector soliton in a spin-orbit coupled spin-1 condensate, *Laser Phys.* **12**, 045501 (2015).
- [19] Gautam S and Adhikari S K, Vector solitons in a spin-orbit-coupled spin-2 Bose-Einstein condensate 2015 *Phys. Rev. A* **91** 063617
- [20] Wen L, Sun Q, Chen Y, Wang D S, Hu J, Chen H, Liu W-M, Juzeliūnas G, Malomed B A and Ji A C, Motion of solitons in one-dimensional spin-orbit-coupled Bose-Einstein condensates 2016 *Phys. Rev. A* **94** 061602(R)
- [21] Vinayagam P S, Radha R, Bhuvaneswari S, Ravisankar R and Muruganandam P, Bright soliton dynamics in spin orbit-Rabi coupled Bose-Einstein condensates 2017 *Comm. Nonlin. Sci. Num. Simul.* **50** 68-76
- [22] Kartashov Y V, Konotop V V and Abdullaev F Kh, Gap solitons in a spin-orbit-coupled Bose-Einstein condensate 2013 *Phys. Rev. Lett.* **111**, 060402
- [23] Zhang Y, Xu Y and Busch T, Gap solitons in spin-orbit-coupled Bose-Einstein condensates in optical lattices 2015 *Phys. Rev. A* **91** 043629
- [24] Kartashov Y V and Konotop V V, Solitons in Bose-Einstein condensates with helicoidal spin-orbit coupling, 2017, *Phys. Rev. Lett.* **118**, 190401.
- [25] Zhu X, Li H, Shi Z, Xiang Y and He Y, Gap solitons in spin-orbit-coupled Bose-Einstein condensates in mixed linear-nonlinear optical lattices, 2017 *J. Phys. B: At. Mol. Opt. Phys.* **50** 155004
- [26] Fialko O, Brand J, and Zülicke U, Soliton magnetization dynamics in spin-orbit-coupled Bose-Einstein condensates, 2012 *Phys. Rev. A* **85** 051605(R)
- [27] Achilleos V, Stockhofe J, Kevrekidis P G, Frantzeskakis D J, and Schmelcher P, Matter-wave dark solitons and their excitation spectra in spin-orbit coupled Bose-Einstein condensates 2013 *EPL* **103** 20002
- [28] Song S W, Wen L, Liu C F, Gou S C, and Liu W M, Ground states, solitons and spin textures in spin-1 Bose-Einstein condensates 2013 *Frontier Phys.* **8** 302-318
- [29] Achilleos V, Frantzeskakis D J, and Kevrekidis P J, Beating dark-dark solitons and Zitterbewegung in spin-orbit-coupled Bose-Einstein condensates 2014 *Phys. Rev. A* **89** 033636
- [30] Cao S, Shan C J, Zhang D W, Qin X Z, and Xu J, Dynamical generation of dark solitons in spin-orbit-coupled Bose-Einstein condensates 2015 *J. Opt. Soc. Am. B* **32** 201-209
- [31] Z. Wu, L. Zhang, W. Sun, X. T. Xu, B. Z. Wang, S. C. Ji, Y. Deng, S. Chen, X. J. Liu, and J. W. Pan, Realization of two-dimensional spin-orbit coupling for Bose - Einstein condensates, *Science* **354**, 83-88 (2016).
- [32] T. Kawakami, T. Mizushima, and K. Machida, Textures of $F = 2$ spinor Bose - Einstein condensates with spin-orbit coupling, *Phys. Rev. A* **84**, 011607 (2011).
- [33] B. Ramachandhran, B. Opanchuk, X. J. Liu, H. Pu, P. D. Drummond, and H. Hu, Half - quantum vortex state in a spin-orbit-coupled Bose - Einstein condensate, *Phys. Rev. A* **85**, 023606 (2012).
- [34] H. Sakaguchi and B. Li, Vortex lattice solutions to the Gross-Pitaevskii equation with spin-orbit coupling in optical lattices. *Phys. Rev. A* **87**, 015602 (2013)
- [35] W. Han, X. F. Zhang, S. W. Song, H. Saito, W. Zhang, W. M. Liu, and S. G. Zhang, Double-quantum spin vortices in $SU(3)$ spin-orbit-coupled Bose gases, *Phys. Rev. A* **94**, 033629 (2016).
- [36] G. J., Conduit, Line of Dirac monopoles embedded in a Bose-Einstein condensate. *Phys. Rev. A* **86**, 021605 (2012).
- [37] C. J. Wu, I. Mondragon-Shem, and X. F. Zhou, Unconventional Bose-Einstein condensations from spin-orbit coupling, *Chin. Phys. Lett.* **28**, 097102 (2011).
- [38] T. Kawakami, T. Mizushima, M. Nitta, and K. Machida, Stable skyrmions in $SU(2)$ gauged Bose - Einstein condensates, *Phys. Rev. Lett.* **109**, 015301 (2012).
- [39] Lobanov V E, Kartashov Y V and Konotop V V, Fundamental, multipole, and half-vortex gap solitons in spin-orbit coupled Bose-Einstein condensates 2014 *Phys. Rev. Lett.* **112** 180403
- [40] Sakaguchi H and Malomed B A, Discrete and continuum composite solitons in Bose-Einstein condensates with the Rashba spin-orbit coupling in one and two dimensions 2014 *Phys. Rev. E* **90** 062922

- [41] Li Y, Luo Z, Liu Y, Chen Z, Huang C, Fu S, Tan H and Malomed B A, Two-dimensional solitons and quantum droplets supported by competing self- and cross-interactions in spin-orbit-coupled condensates 2017 *New J. Phys.* **19** 113043
- [42] Xu Y, Zhang Y P and Zhang C W, Bright solitons in a two-dimensional spin-orbit-coupled dipolar Bose-Einstein condensate 2015, *Phys. Rev. A* **92** 013633
- [43] Li Y, Liu Y, Fan Z, Pang W, Fu S, and Malomed B A, Two-dimensional dipolar gap solitons in free space with spin-orbit coupling, 2017 *Phys. Rev. A* **95** 063613
- [44] Chiao R Y, Garmire E and Townes C H, Self-Trapping of optical beams, 1964 *Phys. Rev. Lett.* **13** 479
- [45] Bergé L, Wave collapse in physics: principles and applications to light and plasma waves 1998 *Phys. Rep.* **303** 259-372
- [46] Sulem C and Sulem P L. *The Nonlinear Schrödinger Equation: Self-Focusing and Wave Collapse* (Springer: New York, 1999).
- [47] Fibich G, *The Nonlinear Schrödinger equation: Singular Solutions and Optical Collapse* (Springer: Cham, Heidelberg, New York, Dordrecht, London, 2015).
- [48] Sakaguchi H, Li B and Malomed B A, Creation of two-dimensional composite solitons in spin-orbit-coupled self-attractive Bose-Einstein condensates in free space 2014 *Phys. Rev. E* **89**, 032920
- [49] Sakaguchi H, Sherman E Ya and Malomed B A, Vortex solitons in two-dimensional spin-orbit coupled Bose-Einstein condensates: Effects of the Rashba-Dresselhaus coupling and the Zeeman splitting, 2016 *Phys. Rev. E* **94**, 032202
- [50] Salasnich, Cardoso W B, and Malomed B A, Localized modes in quasi-two-dimensional Bose-Einstein condensates with spin-orbit and Rabi couplings, 2014 *Phys. Rev. A* **90**, 033629 (2014).
- [51] Sakaguchi H and Malomed B A, One- and two-dimensional solitons in \mathcal{PT} -symmetric systems emulating spin-orbit coupling, 2016 *New J. Phys.* **18** 105005
- [52] Gautam S and Adhikari S K, Vortex-bright solitons in a spin-orbit-coupled spin-1 condensate 2017 *Phys Rev A* **95** 013608
- [53] Kartashov Y V, Torner L, Modugno M, Sherman E Ya, Malomed B A and Konotop V V, 2020 Multidimensional hybrid Bose-Einstein condensates stabilized by lower-dimensional spin-orbit coupling, 2020 *Phys. Rev. Research* **2** 013036
- [54] Malomed B A, Creating solitons by means of spin-orbit coupling 2018 *EPL* **122** 36001
- [55] Zhu Q, Zhang C and Wu B, Exotic superfluidity in spin-orbit coupled Bose-Einstein condensates 2012 *EPL* **100** 50003
- [56] Fallani L, De Sarlo L, Lye J E, Modugno M, Saers R, Fort C and Inguscio M, Observation of dynamical instability for a Bose-Einstein condensate in a moving 1D optical lattice 2004 *Phys. Rev. Lett.* **93** 140406
- [57] Mun J, Medley P, Campbell G K, Marcassa L G, Pritchard D E, and Ketterle W, Phase diagram for a Bose-Einstein condensate moving in an optical lattice 2007 *Phys. Rev. Lett.* **99** 150604
- [58] O. Morsch and M. Oberthaler, Dynamics of Bose-Einstein condensates in optical lattices 2006 *Rev. Mod. Phys.* **78** 179-215
- [59] Baizakov B B, Malomed B A and Salerno M, Multidimensional solitons in periodic potentials 2003 *Europhys. Lett.* **63** 642-648
- [60] Yang J and Musslimani Z H, Fundamental and vortex solitons in a two-dimensional optical lattice, 2003 *Opt. Lett.* **28** 2094-2096
- [61] Musslimani Z H and Yang J, Self-trapping of light in a two-dimensional photonic lattice 2004 *J. Opt. Soc. Amer.* **21** 973-981
- [62] Maytevarunyoo T, Malomed B A, Baizakov B B and Salerno M, Matter-wave vortices and solitons in anisotropic optical lattices 2009 *Physica D* **238** 1439-1448
- [63] Baizakov B B, Malomed B A and Salerno M, Multidimensional solitons in a low-dimensional periodic potential 2004 *Phys. Rev. A* **70**, 053613
- [64] Mihalache D, Mazilu D, Lederer F, Kartashov Y V, Crasovan L-C and Torner L, Stable three-dimensional spatiotemporal solitons in a two-dimensional photonic lattice 2004 *Phys. Rev. E* **70**, 055603(R)
- [65] Chiofalo M L, Succi S, and Tosi M P, Ground state of trapped interacting Bose-Einstein condensates by an explicit imaginary-time algorithm 2000 *Phys. Rev. E* **62** 7438-7444
- [66] Bao W Z and Du Q, Computing the ground state solution of Bose-Einstein condensates by a normalized gradient flow 2004 *SIAM J. Sci. Comp.* **25** 1674-1697
- [67] Bao W and Cai Y, Mathematical theory and numerical methods for Bose-Einstein condensation 2013 *Kinetic and Related Models* **6** 1-135
- [68] Zhang Y-C, Zhou Z-W, Malomed B A and Pu H, Stable solitons in three dimensional free space without the ground state: Self-trapped Bose-Einstein condensates with spin-orbit coupling 2015 *Phys. Rev. Lett.* **115** 253902
- [69] Nistazakis H E, Kevrekidis P G, Malomed B A, Frantzeskakis D J and Bishop A R, Targeted transfer of solitons in continua and lattices 2002 *Phys. Rev E* **66**, 015601(R)
- [70] Davis M C, Carretero-González R, Shi Z, Law K J H, Kevrekidis P G and Anderson B P, Manipulation of vortices by localized impurities in Bose-Einstein condensates 2009 *Phys. Rev. A* **80** 023604
- [71] Liu B, Zhong R, Chen Z, Qin X, Zhong H, Li Y and Malomed B A, Holding and transferring matter-wave solitons against gravity by spin-orbit-coupling tweezers 2020 *New J. Phys.* **22**, 043004

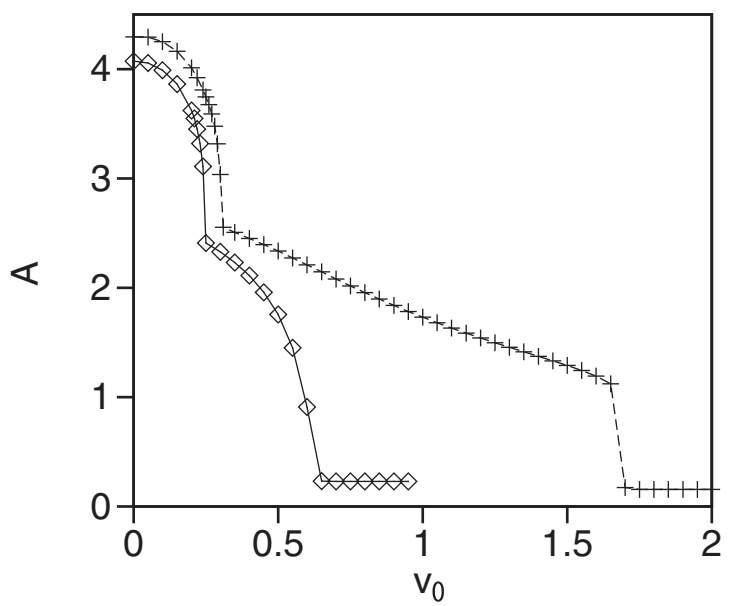
(a)



(b)



(a)



(b)

